Formation of sphalerite and wurtzite ZnO in Pd–Zn alloy after internal oxidation at elevated temperatures

Kei Watanabe · Norihito Sakaguchi · Seiichi Watanabe

Abstract The crystalline structures of zinc oxide (ZnO) formed by the internal oxidation of a Pd–Zn alloy were examined at elevated temperatures. Metastable sphalerite ZnO with a tetrahedral shape preferentially nucleated in the Pd matrix, while plate-like precipitates consisting of a wurtzite ZnO phase preferentially grew at a high temperature. Unique ZnO precipitates with trapezoidal cross-section and consisting of inter-layered sequences with sphalerite ZnO and wurtzite ZnO were also examined at an intermediate temperature. It is inferred that the formation of stacking faults in the sphalerite ZnO is strongly related to the nucleation of the wurtzite-type ZnO sequence.

Introduction

The fabrication of ZnO nanostructures, including nanowires [1–3], nanotubes [4, 5], and nanorods [3, 6, 7] has been studied and well documented by many authors. For the synthesis of ZnO nanostructures, many different approaches have been established, such as chemical vapor deposition [8, 9], thermal evaporation [2, 10–12], pulsed laser deposition [13], solution-phase deposition [5, 14], and direct oxidation of metallic zinc [15, 16]. We have focused on an alternative approach for the fabrication of ZnO nanostructures: internal oxidation of alloys containing solute zinc atoms. Many studies have been conducted on

internally oxidized metal/ZnO systems, for e.g., Ag/ZnO [17] and Pd/ZnO [18–21]. However, almost all of these studies focus on the orientation relationships and atomic structures of metal/ZnO interfaces. In other words, few studies have been conducted on the morphology of ZnO precipitates in the metal matrix. Moreover, the mechanism of nucleation and growth processes has not yet been explained. In this article, we present an electron microscopy study of the morphology and crystallography of ZnO precipitates formed by internal oxidation in a palladium (Pd) matrix. High-resolution transmission electron microscopy (HRTEM) was used to investigate the detailed atomic structure of the precipitates. We also investigated the effect of oxidation temperature on their crystalline structure and morphology. The mechanism of nucleation and growth of ZnO precipitates during internal oxidation is proposed in this article.

Experimental procedure

A palladium rod (purity: 99.99%) was cold rolled down to a thickness of 0.1 mm. The rolled palladium sheet was heated at 1,273 K for 100 h together with a zinc wire (purity: 99.95%) in an evacuated quartz tube to obtain the Pd–Zn alloy. The concentration of zinc in the alloy was 7 at.%. The Pd–Zn sheet was punched out into a disk (diameter: 3 mm), and the disk was electrolytically polished in a solution of 80% acetic acid and 20% perchloric acid at 285 K by using a twin-jet technique. This thin-foil specimen was then internally oxidized for 100 h at 973 to 1,173 K in air. The specimen was finally etched by ion milling for several minutes in order to remove the surface contaminant layer. A high-voltage high-resolution transmission electron microscope (JEM-ARM-1300) was used

K. Watanabe (✉)
Division of Materials Science and Engineering, Graduate School of Engineering, Hokkaido University, Sapporo 060-8628, Japan
e-mail: kei@ufml.caret.hokudai.ac.jp

N. Sakaguchi · S. Watanabe
Center for Advanced Research of Energy and Materials, Faculty of Engineering, Hokkaido University, Sapporo 060-8628, Japan

for HRTEM observations. The spherical and chromatic aberration coefficients of the objective lens of the microscope were 2.65 and 4.1 mm, respectively. The point-to-point resolution measured at a Scherzer defocus of –54 nm and an acceleration voltage of 1,250 kV was 0.118 nm.
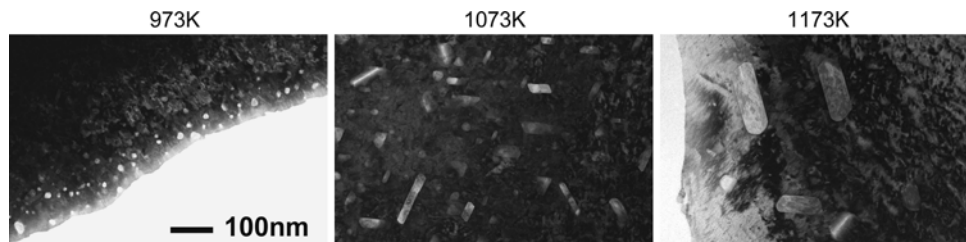
Results and discussion

Microstructures of internally oxidized Pd–Zn alloy

Figure 1 shows the typical microstructures of the Pd–Zn alloy after internal oxidation at several temperatures. The microstructures were observed in the [110] direction of the Pd matrix. Many fine precipitates are found in all specimens. The average size of the precipitates increases with the oxidation temperature, whereas their number density decreases. The precipitates in the specimen oxidized at 973 K are triangular in shape while plate-like precipitates are observed in the specimen oxidized at 1,173 K. At 1,073 K, the triangular and the plate-like precipitates exist together. Moreover, unique trapezoidal precipitates like intermediate between triangular and plate-like are observed. The size of the triangular precipitates is less than 20 nm in length of the side, while the average size of the plate-like precipitates is more than 100 nm in long axis direction. These results suggest that the all of fine precipitates less than 20 nm are triangular in shape and larger than 100 nm are plate-like.

ZnO precipitates with triangular cross-section

Figure 2 shows an HRTEM image and selected-area electron diffraction (SAED) pattern of a typical triangular precipitate. The observations were made in the [110] direction of the Pd matrix. The SAED pattern reveals that the precipitate is a metastable sphalerite ZnO (s-ZnO) phase. It is evident that both the face-centered cubic (FCC) Pd matrix and the s-ZnO precipitate have equivalent crystallographic orientations. Furthermore, the HRTEM image indicates that two equivalent $\{111\}_{Pd}//\{111\}_{s\text{-}ZnO}$ interfaces correspond to two edges of the triangular s-ZnO precipitate. Another edge of the precipitate, which is in an orthogonal direction to the [002] direction, is not well defined and Moire fringes appear there; this suggests that

the interface is not parallel to the viewing direction. Since this inclined interface is equivalent to the other two interfaces, the three-dimensional shape of the s-ZnO precipitate is expected to be a regular tetrahedron with four equivalent $\{111\}_{Pd}//\{111\}_{s\text{-}ZnO}$ interfaces as shown in fig. 3. Such a $\{111\}_{Pd}//\{111\}_{s\text{-}ZnO}$ interface is the polar interface.

In general, metal/ceramics interfaces formed by internal oxidation lie on close-packed planes. In our previous study, it was confirmed that $\{111\}_{Pd}//\{0001\}_{w\text{-}ZnO}$ polar interfaces were preferentially formed by internal oxidation because these interfaces were most stable in Pd/w-ZnO system [21]. Both the $\{0001\}_{w\text{-}ZnO}$ and $\{111\}_{s\text{-}ZnO}$ polar surfaces show an equivalent atomic structure, so that a $\{111\}_{Pd}//\{111\}_{s\text{-}ZnO}$ interface would be a most stable interfacial structure in the Pd/s-ZnO system. In fact, all of the triangular precipitates have same orientation relationships at the interface.

Atomic structure of plate-like precipitates

Figure 4 shows an HRTEM image and SAED pattern of a typical plate-like precipitate. The precipitate is identified as a stable wurtzite ZnO (w-ZnO) phase with orientation relationships of $[110]_{Pd}//[11\bar{2}0]_{w\text{-}ZnO}$ and $(\bar{1}11)_{Pd}//\{0001\}_{w\text{-}ZnO}$. As mentioned above, a $\{0001\}_{w\text{-}ZnO}$ plane is polar and close-packed plane and matched by a close-packed $\{111\}_{Pd}$. Therefore, the $(\bar{1}11)_{Pd}//\{0001\}_{w\text{-}ZnO}$ interface is the lowest energy interfacial structure in Pd/w-ZnO system. It has also been found that ZnO precipitates in internally oxidized Ag–Zn [17] and Pd–Zn [18–21] alloys have the same crystalline structure and orientation relationship. Vellinga et al. had reported that these precipitates have a truncated trigonal shape, dominated by the threefold axis of FCC Ag around the <111> direction [17]. Figure 5 shows a schematic illustration of a plate-like precipitate with large $(111)_{Pd}//\{0001\}_{w\text{-}ZnO}$ interfaces. As reported in previous articles [17–21], it is evident that the interfaces consisting of $(111)_{Pd}//\{0001\}_{w\text{-}ZnO}$ planes are energetically favored in the Pd/w-ZnO system.

ZnO precipitate with multilayered structure

Triangular s-ZnO and the plate-like w-ZnO precipitate simultaneously at 1,073 K. A peculiar change in the shape
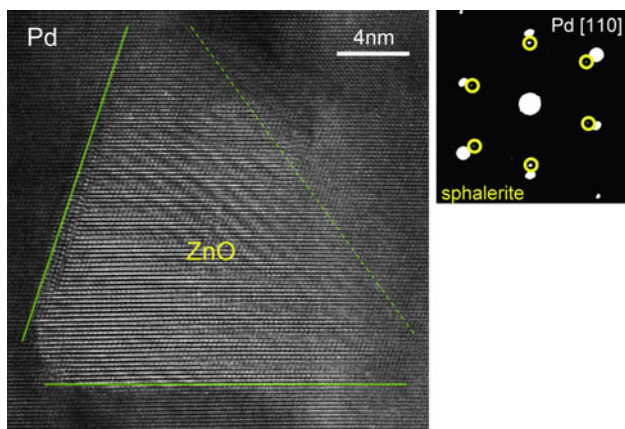

Fig. 1 Bright field TEM images of ZnO precipitates in Pd-7at.%Zn alloy after internal oxidation to 100 h at 973, 1073, and 1173 K

Fig. 2 An HRTEM image and corresponding SAED pattern of typical triangle ZnO precipitate in the Pd–Zn alloy after internal oxidation at 973 K
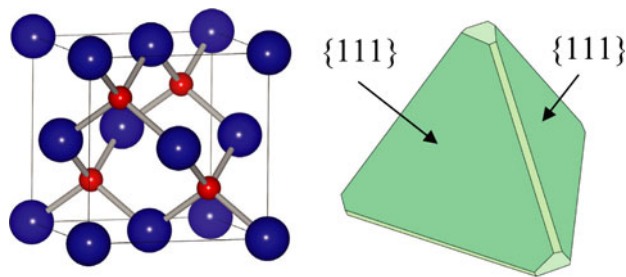

Fig. 3 Atomic structure model and morphology of sphalerite ZnO precipitate

Fig. 5 Atomic structure model and morphology of wurtzite ZnO precipitate

exactly parallel to a $(\bar{1}11)_{s-ZnO}$ basal plane of the tetrahedral s-ZnO. In addition, it is observed that structures different from s-ZnO are periodically introduced parallel to the $(\bar{1}11)_{s-ZnO}$ lattice planes in the ZnO precipitate. Figure 7b shows a magnified HRTEM image of the internal structure of the precipitate. It is found that regions different from s-ZnO corresponded to the w-ZnO phase. Thus, the trapezoidal ZnO precipitate contains a layered structure of s-ZnO/w-ZnO. The orientation relationships of both the ZnO phases are $[110]_{s-ZnO}//[11\bar{2}0]_{w-ZnO}$ and $(\bar{1}11)_{s-ZnO}//\{0001\}_{w-ZnO}$. The $\{0001\}$ surface of w-ZnO is well known as a polar surface, and it is terminated by either zinc or oxygen. The atomic structure of the $(\bar{1}11)_{s-ZnO}$ top surface is as same as that of the $\{0001\}_{w-ZnO}$ polar surface. In other words, the $(\bar{1}11)_{s-ZnO}//\{0001\}_{w-ZnO}$ interface have perfect coherency in its atomic configuration (theoretical lattice misfit is only 0.73%), so that an energy increase due to the formation of the interface can be neglected.

Nucleation and growth of ZnO precipitate during internal oxidation

A unique trapezoidal ZnO precipitate, which has layered structures of s-ZnO/w-ZnO, was examined. The presence of layered structures of s-ZnO/w-ZnO implies that there was a correlation between the triangular s-ZnO and plate-like w-ZnO precipitates. The mechanism of the nucleation and growth of the ZnO precipitates during the internal

of triangular s-ZnO is observed. Figure 6 shows a TEM image of two triangular ZnO precipitates observed in the [110] direction. One of the vertexes of both the triangular precipitates truncated, so that a new interface with $(\bar{1}11)_{Pd}//(\bar{1}11)_{s-ZnO}$ is formed in its place. Thus, the shape of the precipitates appears trapezoidal rather than triangular. An HRTEM image of typical trapezoidal ZnO is shown in Fig. 7. The precipitate, which is originally triangular in shape, attains a trapezoidal shape after one of the vertexes of both the triangular precipitates truncated. The newly formed surface is

Fig. 4 An HRTEM image and corresponding SAED pattern of typical platelet ZnO precipitate in the Pd–Zn alloy after internal oxidation at 1,173 K
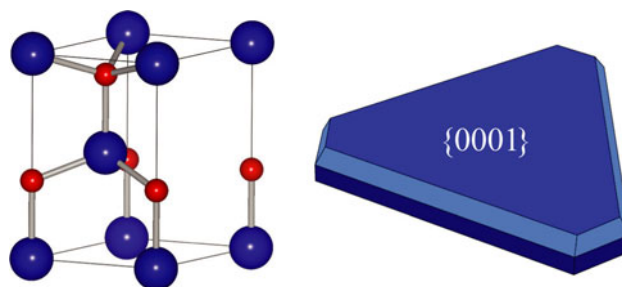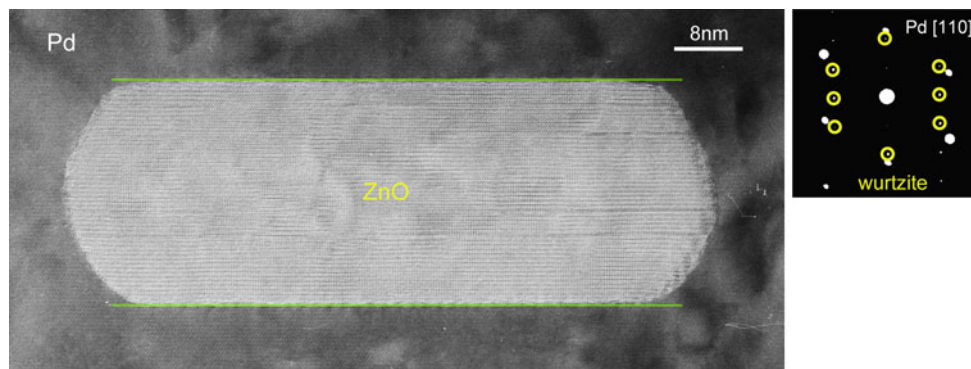
Fig. 6 A bright field TEM image of trapezoidal ZnO precipitates in the Pd–Zn alloy after internal oxidation at 1,073 K
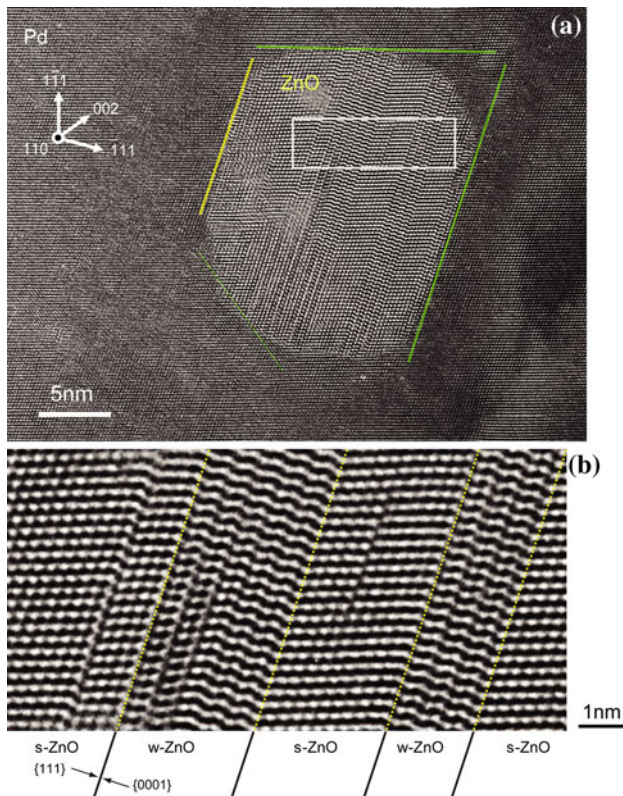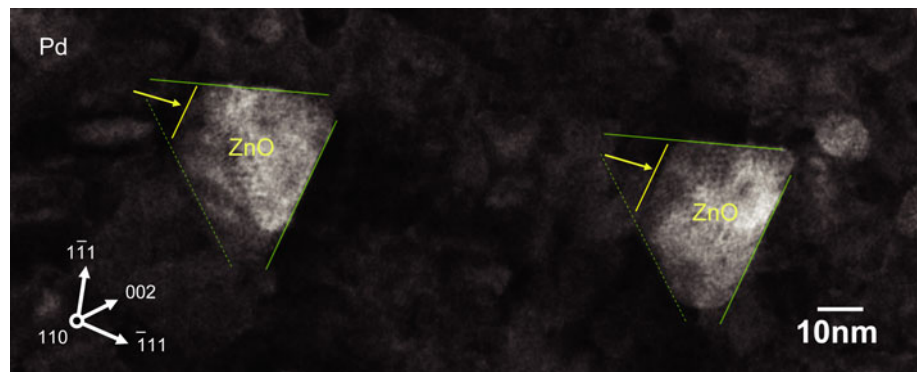

Fig. 7 a An HRTEM image of typical trapezoidal ZnO precipitate, **b** magnified HRTEM image of layered s-ZnO/w-ZnO phases

oxidation process are proposed. Figure 8 shows a schematic illustration of the nucleation and growth processes of ZnO during internal oxidation. The following changes occur in the ZnO precipitate:

(a) Metastable sphalerite ZnO with a tetrahedral shape preferentially nucleates in the Pd matrix. Saib and Bouarissa have calculated the volume energy of ZnO and confirmed that the energy difference between wurtzite and sphalerite is very small while the energy of wurtzite is lower than that of sphalerite [22]. The interfacial energy is predominant over the volume energy, while the size of the precipitate is relatively small during nucleation. Tetrahedral s-ZnO has four equivalent low energy $\{111\}_{Pd}//\{111\}_{s\text{-}ZnO}$ interfaces. The formation of tetrahedral s-ZnO, therefore, minimizes the total free energy of the system, although its volume energy is slightly higher than that of wurtzite ZnO.

(b) As the precipitate grows, the contribution of the volume energy term due to the energy difference between s-ZnO and w-ZnO becomes more important in the total free energy. Since s-ZnO is a metastable phase, it transforms to a stable w-ZnO phase and forms a multi layered structure of s-ZnO/w-ZnO with the interfacial planes of $(111)_{s\text{-}ZnO}//\{0001\}_{w\text{-}ZnO}$. One of the vertexes of tetrahedral s-ZnO in a direction vertical to the $(111)_{s\text{-}ZnO}$ plane truncates and a new interface with $(111)_{Pd}//(111)_{s\text{-}ZnO}$ is formed.

(c) Since the s-ZnO phase completely transforms to w-ZnO, the ZnO precipitate preferentially grows while retaining the $(111)_{Pd}//\{0001\}_{w\text{-}ZnO}$ polar interfaces. Therefore, most of the large precipitates have a plate-like shape with a wurtzite crystalline structure.

In Figs. 2 and 4, since there was no strain contrast due to the misfit dislocation formed by interfacial mismatch, $\{111\}_{Pd}//\{111\}_{s\text{-}ZnO}$ and $(111)_{Pd}//\{0001\}_{w\text{-}ZnO}$ interfaces would be properly incoherent. Some conclusions were carried out in the references 18–21 that no misfit dislocation was observed at $(111)_{Pd}//\{0001\}_{w\text{-}ZnO}$ interfaces. This indicates that the strain energy term due to the interfacial mismatch can be neglected for the phase transformation.

Formation of sphalerite ZnO has been found as a nucleus for wurtzite ZnO tetrapods by thermal vapor deposition [23]. In the present study, these two ZnO polymorphs can coexist under ambient conditions in form of precipitates produced by internal oxidation of Pd–Zn alloy.

It is expected that nucleation of w-ZnO in s-ZnO occurred along to $\{111\}_{s\text{-}ZnO}$ plane and introduced a $\{111\}_{s\text{-}ZnO}//\{0001\}_{w\text{-}ZnO}$ interface. Since the s-ZnO has four equivalent $\{111\}$ planes, i.e. $(\bar{1}11)$, $(1\bar{1}1)$, $(\bar{1}1\bar{1})$, and $(1\bar{1}\bar{1})$ in some cases, w-ZnO phases can nucleate with different variants in one precipitate. In this case, these two w-ZnO domains contact each other and form a grain boundary in the

Fig. 8 A schematic illustration of the nucleation and growth processes of ZnO during internal oxidation
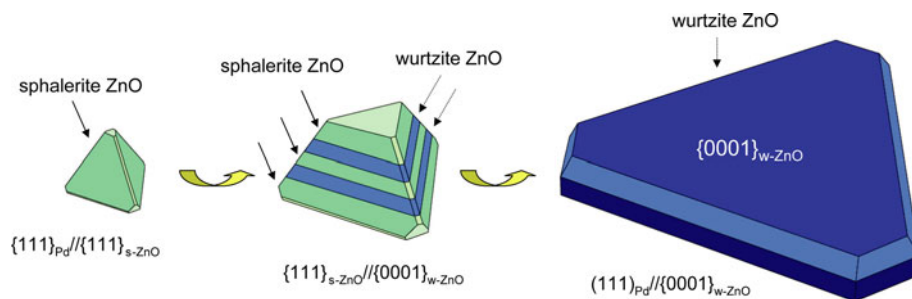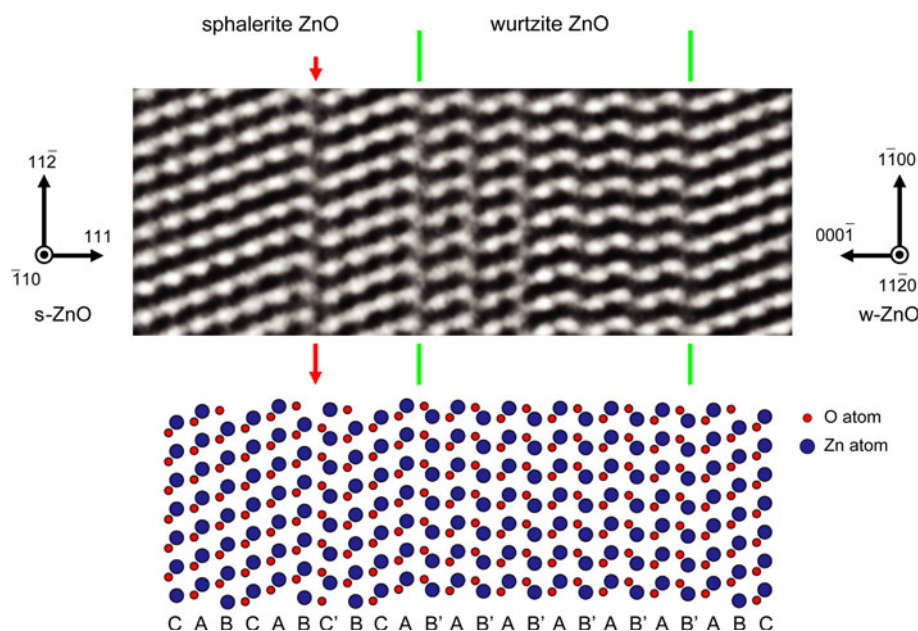

Fig. 9 An HRTEM image and corresponding atomic model of layered s-ZnO/w-ZnO phases

precipitate. However, this boundary is expected to have higher energy than other interfaces such as the {111}$_{s-ZnO}$//{0001}$_{w-ZnO}$. As the growth of the w-ZnO domains, the elongation of the grain boundary raises a total energy of the system due to its high grain boundary energy. The phase transformation from s-ZnO to w-ZnO is then stopped when the energy profit due to the volume energy difference balances with the energy increment by the elongation of the grain boundary. Such precipitates have often observed in internally oxidized Ag–Zn and Pd–Zn alloys [17, 19]

Mechanism of phase transformation from sphalerite ZnO to wurtzite ZnO

During the growth of the tetrahedral s-ZnO precipitate, it is expected that the layered w-ZnO phase would be introduced in the precipitate with the interfacial planes of (111)$_{s-ZnO}$//{0001}$_{w-ZnO}$. Both the s-ZnO and w-ZnO phases have almost the same atomic structures, while the former has FCC stacking ("ABCABC") of (111)$_{s-ZnO}$ planes, the latter has hexagonal close-packed (HCP) stacking ("AB'AB'AB'") of (0001)$_{w-ZnO}$ planes. Due to

their almost same atomic structure, these two phases are closely related to the stacking faults formed in the s-ZnO precipitate. Figure 9a and b shows an HRTEM image of a stacking fault in the s-ZnO phase and the corresponding atomic model, respectively. The larger blue circles indicate Zn atoms, while the smaller red circles indicate O atoms. The stacking fault, indicated by an arrow, is formed parallel to the (111)$_{s-ZnO}$ planes. From an analysis of the atomic model of the stacking fault in the sphalerite structure, it is apparent that the direction of the Zn–O dumbbells changed to minimize the bonding energies between oxygen and adjacent zinc atoms. The local atomic structure around the stacking fault ("BC'B" stacking in the figure) is the same as that of wurtzite ZnO. In this case, the interfaces between s-ZnO and w-ZnO always correspond to (111)$_{s-ZnO}$//{0001}$_{w-ZnO}$. Therefore, it is suggested that the formation of stacking faults in s-ZnO is strongly related to the nucleation of the layered w-ZnO phase.

During the growth of ZnO precipitate in the Pd matrix, ZnO should be subjected to a stress from surrounding Pd. In the Pd/ZnO system, elastic modulus of Pd is greater than that of ZnO, so that the dislocations preferentially is

formed and slip in s-ZnO to reduce the strain around the precipitates. A dislocation would easily be separated into partial dislocations in the s-ZnO and the distance between partial dislocations would be extended from end to end of the precipitates because of low stacking fault energy of s-ZnO. After a partial dislocation slipped through the precipitate, stacking fault is left in the s-ZnO. In Fig. 4, one can see many stacking faults remaining in the w-ZnO precipitate. Some of the stacking faults were terminated interior of the grain and partial dislocation remained there. It is speculated that the formation of the stacking faults resulted from the phase transformation from s-ZnO to w-ZnO.

Conclusion

The crystalline structures of ZnO formed by the internal oxidation of a Pd–Zn alloy were examined at several temperatures. A metastable sphalerite ZnO with a tetrahedral shape preferentially nucleates in the Pd matrix, while the plate-like precipitates consisting of a wurtzite ZnO phase preferentially grows at a high temperature. Tetrahedral s-ZnO and plate-like w-ZnO precipitate simultaneously at 1,073 K. Unique trapezoidal ZnO precipitates having layered structures of s-ZnO/w-ZnO were examined. Since the local atomic structure around the stacking fault is the same as that of wurtzite ZnO, the formation of stacking faults in s-ZnO is strongly related to the nucleation of the layered w-ZnO phase.

References

1. Tseng YK, Lin IN, Liu KS, Lin TS, Chen IC (2003) J Mater Res 18:714
2. Wan Q, Lin CL, Yu XB, Wang TH (2004) Appl Phys Lett 84:124
3. Zhang WD, Zhang WH, Ma XY (2009) J Mater Sci 44:4677. doi: 10.1007/s10853-009-3716-0
4. Xing YJ, Xi ZH, Xue ZQ, Zhang XD, Song JH, Wang RM, Xu J, Song Y, Zhang SL, Yu DP (2003) Appl Phys Lett 83:1689
5. Hu JQ, Bando Y (2003) Appl Phys Lett 82:1401
6. Gao PX, Ding Y, Wang ZL (2003) Nano Lett 3:1315
7. Umar A, Kim SH, Suh EK, Hahn YB (2007) Chem Phys Lett 440:110
8. Yang JL, An SJ, Park WI, Yi GC, Choi W (2004) Adv Mater 16:1661
9. Ng HT, Han J, Yamada T, Nguyen P, Chen YP, Meyyappan M (2004) Nano Lett 4:1247
10. Huang Y, He J, Zhang Y, Dai Y, Gu Y, Wang S, Zhou C (2006) J Mater Sci 41:3057. doi:10.1007/s10853-006-6978-9
11. Li Y, Li WF, Xu G, Ma XL, Cheng HM (2008) J Mater Sci 43:1711. doi:10.1007/s10853-007-2344-9
12. Wan Q, Li QH, Chen YJ, Wang TH, He XL, Li JP, Lin CL (2004) Appl Phys Lett 84:3654
13. Zhang YF, Russo RE, Mao SS (2005) Appl Phys Lett 87:133115-1
14. Tian ZR, Voigt JA, Liu J, Mckenzie B, Mcdermott MJ, Rodriguez MA, Konishi H, Xu H (2003) Nat Mater 2:821
15. Yang Q, Tang K, Zuo J, Qian Y (2004) Appl Phys A 79:1847
16. Chen YQ, Jiang J, He ZY, Su Y, Cai D, Chen L (2005) Mater Lett 59:3280
17. Vellinga WP, De Hosson JTM (1997) Acta Mater 45:933
18. Ichimori T, Katoh T, Ichinose H, Ito K, Ishida Y (1996) In: Proceedings of JIMIS-8, Japan Institute of Metal, pp 359–362
19. Groen HB, De Hosson JTM (1998) Scripta Mater 38:769
20. Murakami K, Saito M, Takuma E, Ichinose H (2003) J Electron Microsc 52:27
21. Sakaguchi N, Suzuki Y, Watanabe K, Iwama S, Watanabe S, Ichinose H (2008) Philos Mag 88:1493
22. Siab S, Bouarissa N (2007) Phys Stat Sol (b) 244:1063
23. Ding Y, Wang ZL, Sun T, Qiu J (2007) Zinc-blende ZnO and its role in nucleating wurtzite tetrapods and twinned nanowires. Appl Phys Lett 90:153510-1